The Astrophysical Journal Letters, 974:L36 (12pp), 2024 October 20 https://doi.org/10.3847/2041-8213/ad7eb8

AT2023vto: An Exceptionally Luminous Helium Tidal Disruption Event from a Massive Star

Harsh Kumar[1,2], Edo Berger[1,2], Daichi Hiramatsu[1,2], Sebastian Gomez[3], Peter K. Blanchard[1], Yvette Cendes[1,4], K. Azalee Bostroem[5], Joseph Farah[5,6], Estefania Padilla Gonzalez[5,6], D. Andrew Howell[5,6], Curtis McCully[5], Megan Newsome[5,6], and Giacomo Terreran[5]

[1] Center for Astrophysics | Harvard & Smithsonian, 60 Garden Street, Cambridge, MA 02138-1516, USA
[2] The NSF AI Institute for Artificial Intelligence and Fundamental Interactions, USA
[3] Space Telescope Science Institute, 3700 San Martin Drive, Baltimore, MD 21218, USA
[4] Department of Physics, University of Oregon, Eugene, OR 97403, USA
[5] Las Cumbres Observatory, 6740 Cortona Drive, Suite 102, Goleta, CA 93117-5575, USA
[6] Department of Physics, University of California, Santa Barbara, CA 93106-9530, USA
Received 2024 August 2; revised 2024 September 13; accepted 2024 September 14; published 2024 October 17

Abstract

We present optical/UV observations and the spectroscopic classification of the transient AT2023vto as a tidal disruption event (TDE) at $z = 0.4846$. The spectrum is dominated by a broad blueshifted He II λ4686 emission line, classifying it as a member of the TDE-He class. The light curve exhibits a persistent blue color of $g - r \approx -0.4$ mag, long rise, and decline timescale, with a large peak absolute magnitude of $M_g \approx -23.2$, making it the most luminous of the classical optical TDEs (H, H+He, He) discovered to date by about 1.5 mag. We identify the host galaxy of AT2023vto in archival Pan-STARRS images and find that the transient is located at the galaxy center. Modeling the light curves of AT2023vto, we find that it resulted from the disruption of a $\approx 8\,M_\odot$ star by a $\approx 10^7 M_\odot$ supermassive black hole. The star mass is about 5 times larger than the highest star masses previously inferred in TDEs, and the black hole mass is at the high end of the distribution. AT2023vto is comparable in luminosity and timescale to some putative TDEs (blue featureless continuum), as well as to the mean of a recently identified population of ambiguous nuclear transients (ANTs). ANTs have been speculated to arise from tidal disruptions of massive stars, perhaps in active galactic nuclei, and AT2023vto may represent a similar case to ANTs but in a dormant black hole, thereby bridging the TDE and ANT populations. We anticipate that the Rubin Observatory/LSST will uncover similar luminous TDEs to $z \sim 3$.

Unified Astronomy Thesaurus concepts: Tidal disruption (1696); Time domain astronomy (2109); Transient sources (1851); Optical astronomy (1776); AB photometry (2168)

Materials only available in the online version of record: machine-readable table

1. Introduction

Over the past decade, the observed population of tidal disruption events (TDEs; M. J. Rees 1988; C. R. Evans & C. S. Kochanek 1989) has grown rapidly to tens of events. The observed TDE population appears to be dominated by the disruption of stars spanning ~ 0.1–$2\,M_\odot$ by supermassive black holes (SMBHs) spanning $\sim 10^{5.5}$–$10^{7.5}\,M_\odot$ (B. Mockler et al. 2019; S. van Velzen et al. 2021a; M. Nicholl et al. 2022; S. Gomez et al. 2023; E. Hammerstein et al. 2023; Y. Yao et al. 2023). Spectroscopic observations have also demonstrated a diversity of TDEs, with spectra dominated by broad hydrogen lines (TDE-H), a mix of hydrogen and helium (TDE-H+He), and only helium lines (TDE-He); e.g., I. Arcavi et al. (2014), S. Gezari (2021), M. Nicholl et al. (2022), P. Charalampopoulos et al. (2022), E. Hammerstein et al. (2023), and Y. Yao et al. (2023). These emission lines often exhibit velocity shifts, indicating outflowing gas driven by intense radiation pressure near the black hole, with velocities ranging from hundreds to $\sim 10^4$ km s^{-1} (T. Hung et al. 2019; M. Nicholl et al. 2019; P. Charalampopoulos et al. 2022; T. Wevers et al. 2022). Thus TDEs provide an excellent laboratory for the study of accretion and outflows around otherwise dormant SMBHs and a census of their demographics.

Along with the growing population of spectroscopically classified ("classical") optical TDEs, other putative or potentially related events have also been recognized in wide-field optical surveys. These include events with similar luminosities, timescales, colors, and an origin in host galaxy nuclei but lacking any spectral features (termed "featureless" TDEs; E. Hammerstein et al. 2023), as well as events with a contentious origin such as ASASSN-15lh, which has been argued to be either a TDE (G. Leloudas et al. 2016) or a superluminous supernova (SN; P. J. Brown et al. 2016; S. Dong et al. 2016), or the very luminous transient AT2021lwx, whose origin is unclear but has been speculated to potentially be a TDE (B. M. Subrayan et al. 2023). Relatedly, a new class of nuclear transients, dubbed ambiguous nuclear transients (ANTs; A. J. Drake et al. 2011; E. Kankare et al. 2017; J. M. M. Neustadt et al. 2020; T. W. S. Holoien et al. 2022; P. Wiseman et al. 2024), has also been recognized. ANTs are loosely defined as transients coinciding with their host galaxy nuclei, which do not resemble spectroscopic SNe, TDEs, or normal active galactic nuclei. Some ANTs are ~ 1–2 orders of magnitude more luminous than classical TDEs and exhibit much longer durations (J. T. Hinkle et al. 2024; P. Wiseman et al. 2024), and it has been speculated that they may represent tidal disruptions of massive stars, much beyond

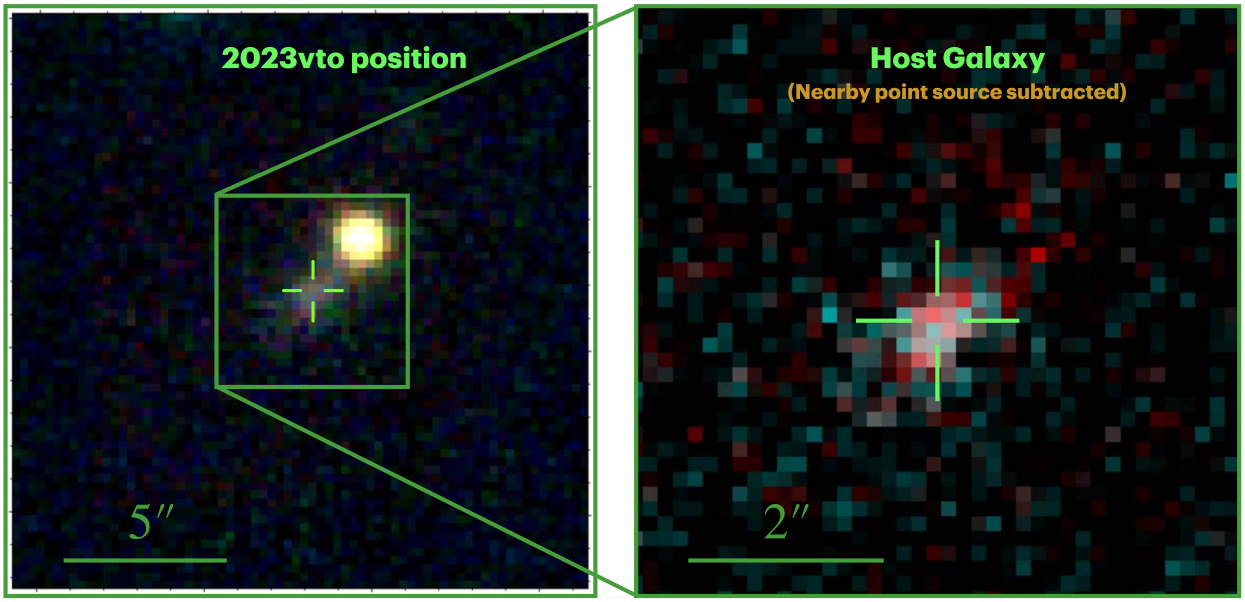

Figure 1. Archival PS-DR1 images centered on the location of AT2023vto. There are two distinct sources within a few arcseconds of the location of the transient; the fainter extended source directly underlies the position of AT2023vto and is its host galaxy (the brighter point source is a likely foreground star). Right: a zoomed-in image with the point source subtracted. We find that AT2023vto coincides with the center of its host galaxy, supporting its TDE origin.

the typical solar mass stars in classical TDEs (P. Wiseman et al. 2024); in this scenario it remains unclear why disruptions of such massive stars would lead to distinct optical spectra.

Against this backdrop, here we present the study of the most luminous classical TDE to date—AT2023vto—with a peak luminosity exceeding the median of the TDE population by nearly 2 orders of magnitude, but comparable to the median for the ANT population, and which exhibits a broad and blueshifted He II line characteristic of the TDE-He class and is distinct from ANTs. The high luminosity of AT2023vto points to the disruption of a massive star ($\sim 9\,M_\odot$), and it potentially represents a bridge between the classical TDE and luminous ANT populations. The Letter is arranged as follows. In Section 2, we summarize the discovery and multiwavelength follow-up observations of AT2023vto and its host galaxy. In Section 3 we demonstrate that AT2023vto is a a classical TDE. In Section 4, we model the UV/optical light curve to determine the properties of AT2023vto and show that it resides in a unique part of the star mass—the black hole mass phase space of TDEs. We compare the observed and inferred properties of AT2023vto to the TDE population and other potentially related phenomena (e.g., ANTs) in Section 5 and summarize the key results and implications in Section 6. Throughout this work, we use standard Planck18 FlatLambdaCDM cosmology (Planck Collaboration et al. 2020) with Hubble constant $H_0 = 67.4 \pm 0.5$ km s^{-1} Mpc^{-1} and matter density parameter $\Omega_m = 0.315 \pm 0.007$. We estimated a luminosity distance of $d_L = 2812.7 \pm 0.3$ Mpc using a redshift $z = 0.48463 \pm 0.00004$ (see Section 2.4) for AT2023vto.

2. Discovery and Observations

2.1. Discovery

AT2023vto was first detected on 2023 September 9 by the Zwicky Transient Facility (ZTF; internal name: ZTF23abcvbqq) at R.A. $= 00^{h}24^{m}34\overset{s}{.}71$, decl. $= +47°13'21\overset{''}{.}55$ (J2000) with a magnitude of $m_g = 20.98 \pm 0.33$ (C. Fremling 2023). On 2023 November 21, F. Poidevin et al. (2023) obtained an optical spectrum of the transient and classified it as a Type II superluminous SN (SLSN-II) at $z = 0.48463$, based on its luminosity and the tentative identification of a faint Hβ emission feature. Below, we show that while the redshift is correct, the identification of Hβ is likely erroneous (or the spectrum has evolved significantly), and AT2023vto is not an SLSN-II but a TDE.

2.2. Host Galaxy

Inspection of the Pan-STARRS Data Release 1 (PS-DR1) archival images reveals two sources within a few arcseconds of the location of AT2023vto; see Figure 1. The brighter, point-like source is well resolved from the location of AT2023vto (offset by $2\overset{''}{.}3$), while the fainter, extended source directly underlies the position of AT2023vto. As shown in Figure 1, subtracting the nearby source using the point-spread function (PSF) profile determined from the images results in clean residuals, implying it is a likely foreground star. We identify the extended source as the host galaxy of AT2023vto, with the following magnitudes determined from the PS-DR1 images after subtracting the nearby point source: $m_g = 22.60 \pm 0.18$, $m_r = 21.33 \pm 0.16$, $m_i = 20.54 \pm 0.22$, $m_z = 19.99 \pm 0.23$, and $m_y = 20.03 \pm 0.19$. This indicates that contamination from host galaxy light in UV and blue optical bands is negligible. At the redshift of the galaxy, the corresponding absolute magnitudes are $M_g = -20.07 \pm 0.18$, $M_r = -21.34 \pm 0.16$, $M_i = -22.13 \pm 0.22$, $M_z = -22.68 \pm 0.23$, and $M_y = -22.64 \pm 0.19$.

We model the host spectral energy distribution with the `Prospector` code (J. Leja et al. 2017) to estimate its stellar mass and hence to infer its associated SMBH mass. We use an exponential star formation history and include the metallicity and dust contributions as free parameters. The resulting best-fit SED model is shown in Figure 2. We find a stellar mass of $\log(M_{\rm gal}/M_\odot) = 10.74 \pm 0.24$ and a metallicity of $\log(Z) = -0.11^{+0.38}_{-0.28}$. Using the galaxy stellar mass to black hole mass relation of $\log(M_{\rm BH}/M_\odot) = 6.70 + 1.61 \times \log(M_{\rm gal}/3 \times 10^{10} M_\odot)$

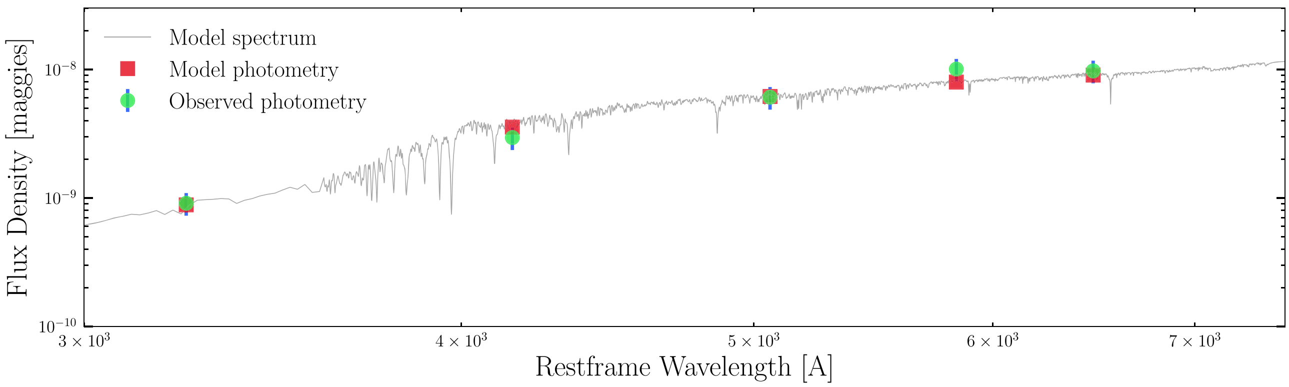

Figure 2. Spectral energy distribution of the host galaxy of At2023vto (green points) along with the best-fit model from `Prospector` (red points and gray curve). The host photometry has been measured from PS-DR1 images with the nearby point source subtracted (see Figure 1).

(J. E. Greene et al. 2020; Z. Q. Zhou et al. 2021), we estimate a black hole mass of $\log(M_{\rm BH}/M_{\odot}) = 7.12 \pm 0.38$.

2.3. Imaging Observations

Motivated by the initial SLSN-II classification, we began follow-up observations of AT2023vto with the Sinistro cameras on the network of Las Cumbres Observatory (LCO; T. M. Brown et al. 2013) 1 m telescopes in the U, B, V, g, r bands through the Global Supernova Project (D. A. Howell & Global Supernova Project 2017). LCO photometry was performed with PSF fitting using `lcogtsnpipe`[7] (S. Valenti et al. 2016), a PyRAF-based photometric reduction pipeline. The U-, B-, V-band data were calibrated to Vega (P. B. Stetson 2000) magnitudes using standard fields observed on the same night by the same telescope as AT2023vto, while the g-, r-, and i-band data were calibrated to AB magnitudes using the 9th Data Release of the AAVSO Photometric All-Sky Survey (A. A. Henden et al. 2016). All photometric measurements in the LCO g and r bands were obtained after image subtraction with the in-house zogy algorithm python pipeline (B. Zackay et al. 2016). We did not perform image subtraction in the U, B, and V bands due to negligible host contamination in these blue bands.

We additionally obtained publicly available data from ZTF (E. Bellm 2014; E. C. Bellm et al. 2019), ATLAS (J. L. Tonry et al. 2018), and the Neil Gehrels Swift Observatory (N. Gehrels et al. 2004). We obtained the ZTF g- and r-band data through the Automatic Learning for the Rapid Classification of Events broker (F. Förster et al. 2021). The data span from 2023 September 9 to December 12 in the g band and from 2023 September 15 to 2024 January 2 in the r band.

ATLAS observed AT2023vto in the c and o bands, and we obtained the photometry from the ATLAS forced photometry server (L. Shingles et al. 2021), selecting all detections with a signal-to-noise ratio of $\geqslant 5$. To reduce scatter from the individual exposures, we determined a weighted median of all observations in 2 days bins. The data spanned 2023 September 15–December 13 in the c band and 2023 September 25–December 15 in the o band.

Swift observations were obtained with the UV/Optical Telescope (UVOT; P. W. A. Roming et al. 2005) in all six filters (UVW2, UVM2, UVW1, U, B, and V). The observation commenced on 2023 December 3 (Target ID 16397), with four visits up to December 16. We obtained three additional observations from 2024 May 25 to June 2 for reference templates and performed aperture photometry with `Swift_host_subtraction`,[8] following the standard procedures described in P. J. Brown et al. (2009, 2014).

All photometric measurements reported in this work are in AB magnitudes and corrected for Galactic extinction (see Table 1), with $E(B-V) = 0.088$ mag (E. F. Schlafly & D. P. Finkbeiner 2011), assuming the E. L. Fitzpatrick (1999) reddening law with $R_V = 3.1$. Given the very blue colors and lack of host galaxy Na I D absorption lines in the spectrum (see below), the host galaxy extinction is expected to be negligible; this is verified independently with `MOSFiT` modeling in Section 4.

The resulting multiband light curve is shown in Figure 3. We find that the light curve exhibits a slow rise for ≈50 days postdiscovery, rising by ≈2 mag in the g band and peaking at $m_g = 18.61 \pm 0.13$, or $M_g \approx -23.2$, mag on MJD = 60245.3 (which we define as phase = 0). The light curve then declines slowly, taking ≈50 days to reach half of its peak brightness. Equally important, the light curve exhibits a persistent blue $g-r$ color of -0.43 ± 0.10 mag throughout its evolution (with a possible slight reddening beyond MJD of about 60,300).

Table 1
Photometry of AT2023vto

MJD	Filter	Magnitude ± e_magnitude (AB)	Telescope
60170.40884	r	>20.55	ZTF
60173.33883	r	>20.4	ZTF
60173.47114	g	>20.47	ZTF
60178.42973	g	>20.47	ZTF
60180.40827	g	>19.18	ZTF
60182.34443	r	>20.44	ZTF
60182.42775	g	>20.28	ZTF
60184.42790	g	>20.32	ZTF
60184.47108	r	>20.46	ZTF
60186.35961	r	>19.53	ZTF

Note. Magnitudes are corrected for Galactic extinction in the direction of AT2023vto and are in the AB system. The full version of this table is available in machine-readable format in the online journal. A portion is shown here for guidance regarding its form and function.

(This table is available in its entirety in machine-readable form in the online article.)

[7] https://github.com/LCOGT/lcogtsnpipe

[8] https://github.com/gterreran/Swift_host_subtraction/tree/main

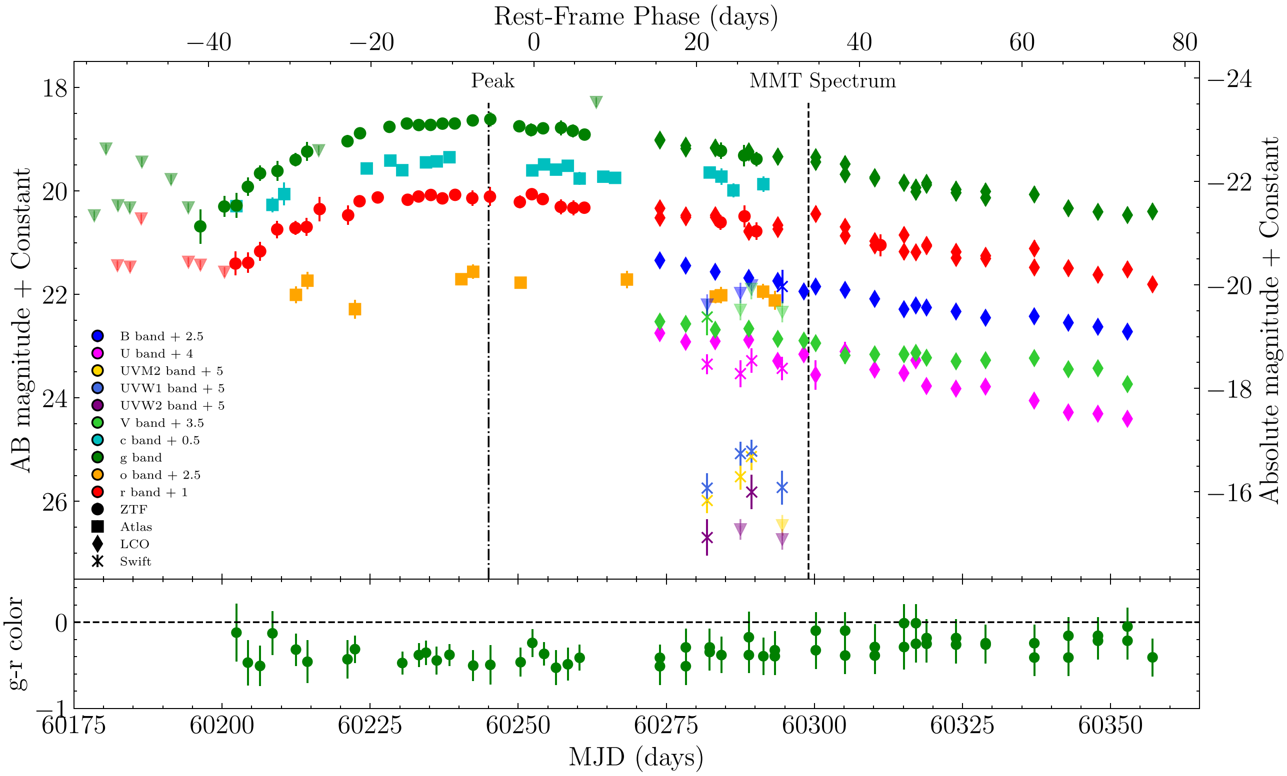

Figure 3. Optical/UV light curves of AT2023vto. The magnitudes are corrected for Galactic extinction. Photometry has been obtained from ZTF (circles), ATLAS (squares), LCO (diamonds), and Swift (crosses). AT2023vto peaks in the g band about 50 days postdiscovery with a peak absolute magnitude of $m_g \approx -23.2$. The $g - r$ color is blue (≈ -0.4 mag) and does not evolve significantly during the rise and decline phase of the light curve for about 155 days, typical of TDEs.

2.4. Optical Spectroscopy

We obtained an optical spectrum of AT2023vto with the Binospec spectrograph (D. Fabricant et al. 2019) on the MMT 6.5 m telescope on 2023 December 21, corresponding to an observed phase of ≈54 days (rest-frame phase of ≈37 days). We analyzed the spectrum using standard IRAF routines in the `twodspec` package. The spectrum was bias subtracted and flat fielded, the sky background was modeled and subtracted from the 2D image, and the 1D spectra were optimally extracted, weighing by the inverse variance of the data. A wavelength calibration was applied using an arc lamp spectrum taken directly after the science image. Relative flux calibration was applied to the spectrum using a standard star taken close to the observation time.

The spectrum, shown in Figure 4, reveals a strong Mg II absorption doublet from the host galaxy, which gives a redshift of $z = 0.48463 \pm 0.00004$ (see inset of Figure 4). Additionally, we detect a broad emission feature centered at a rest-frame wavelength of ≈4511 Å, which corresponds most closely to He II λ4686. Since the earlier spectrum used for the initial classification (observed phase of 26 days; F. Poidevin et al. 2023) is not publicly available, we cannot determine if the broad feature we observe was misidentified as Hβ or whether the spectrum has evolved from being dominated by Hβ to He II λ4686; such a transition was claimed for the TDE AT2017eqx (M. Nicholl et al. 2019) but over a much longer timescale of ≈100 days compared to only ≈30 days in this case. Regardless, based on our MMT spectrum, we reclassify AT2023vto as a TDE-He event.

Fitting the emission feature with a skewed Gaussian profile, we find that it peaks at $\lambda = 4511 \pm 48$ Å, with a FWHM of $v_{\rm FWHM} = (3.90 \pm 0.3) \times 10^4$ km s^{-1} and skewness of $\alpha = 1.73 \pm 0.83$ (see inset in Figure 4). The velocity shift of the line center relative to the rest wavelength is $v_{\rm He} = (-1.11 \pm 0.3) \times 10^4$ km s^{-1}, which is large but not unprecedented for TDE-He (T. Hung et al. 2019; see Section 5). If the observed feature was Hβ, the resulting velocity shift would be $\approx -2.1 \times 10^4$ km s^{-1}, which is 1 order of magnitude larger[9] than observed in other TDEs (P. Charalampopoulos et al. 2022). A blackbody fit to the continuum (with the emission feature subtracted) gives a temperature of $T_{\rm BB} = 19{,}926 \pm 211$ K. We note that this is likely a lower limit as the spectral peak is blueward of the observed wavelength range of our spectrum. The blueshifted, asymmetric He II emission line is similar to those previously seen in emission lines of TDEs and is likely caused by redshifting of the scattered line photons in the expanding outflow (N. Roth & D. Kasen 2018).

2.5. Radio Observations

Following our identification of AT2023vto as a TDE, we obtained radio observations with the Karl G. Jansky Very Large Array (VLA) on 2024 June 19 (284 days post-optical discovery) using Director's Discretionary Time (Program ID 24A-479, PI: Cendes). We observed AT2023vto in the C band (4–8 GHz) using the primary calibrator 3C147 and the secondary calibrator J2355+4950. We processed the VLA data using standard data reduction procedures in the Common Astronomy Software Application package (J. P. McMullin et al. 2007), using `tclean` on the calibrated measurement set

[9] Or in Type II SNe (J. P. Anderson et al. 2014).

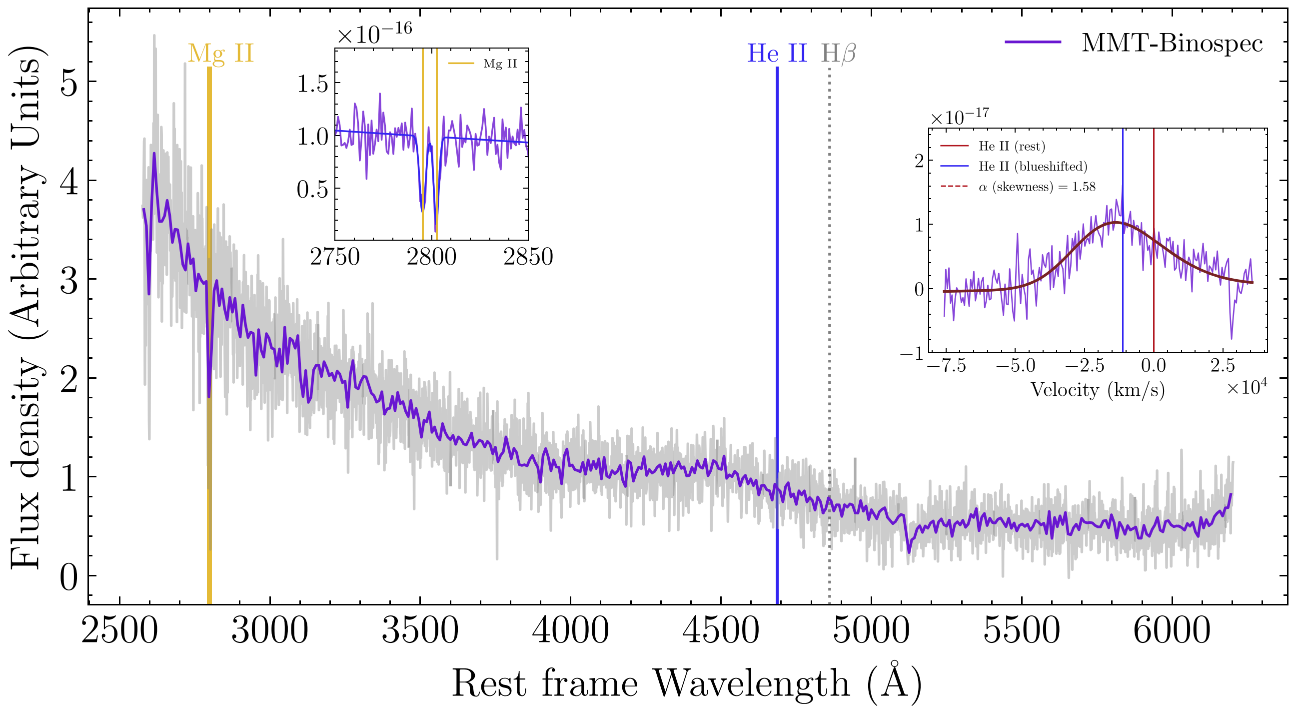

Figure 4. MMT/Binospec optical spectrum of AT2023vto obtained at a phase of +54 days, shown in rest-frame wavelength (the purple line is binned by a factor of 5). The narrow Mg II absorption doublet indicates a redshift of $z = 0.48463 \pm 0.00004$ (left inset). We find a single broad emission feature centered at 4511 Å, with $v_{\rm FWHM} \approx 3.90 \times 10^4$ km s^{-1} and a blueshift of $\approx 1.11 \times 10^4$ km s^{-1} relative to the rest wavelength of He II λ4686 (right inset). This feature is inconsistent with Hβ (dotted vertical line), indicating a TDE-He classification.

available in the NRAO archive, with Briggs weighting. We do not detect a radio source at the location of AT2023vto, with a 3σ upper limit of $F_\nu \approx 16.5\ \mu$Jy, corresponding to a luminosity limit of $\nu L_\nu \lesssim 9 \times 10^{38}$ erg s^{-1}. This limit is not constraining in the context of TDEs with nonrelativistic outflows (K. D. Alexander et al. 2020; Y. Cendes et al. 2024) but rules out the luminosities seen in TDEs with on-axis relativistic jets (E. Berger et al. 2012; B. A. Zauderer et al. 2013; G. C. Brown et al. 2017). Future observations will determine if AT2023vto exhibits late-time radio emission as seen in a substantial fraction of TDEs (Y. Cendes et al. 2024).

2.6. X-Ray Observations

We analyzed Swift X-Ray Telescope (XRT; 0.3–10 keV) observations obtained along with the UVOT observations (phase of 32–49 days). No emission was detected at the location of AT2023vto, and we estimate a 3σ upper limit using the Swift-XRT web tool[10] (P. A. Evans et al. 2007, 2009). With a Milky Way H I column density of 7.63×10^{20} cm^{-2} (HI4PI Collaboration et al. 2016)[11] and assuming a power-law spectrum with a photon index of 2, the stacked source count rate limit is converted[12] to an unabsorbed flux limit of $F_{\rm X} \lesssim 9.2 \times 10^{-13}$ erg s^{-1} cm^{-2}, corresponding to a luminosity limit of $L_{\rm X} \lesssim 8.7 \times 10^{44}$ erg s^{-1}. This limit is not particularly constraining relative to the majority of TDEs, which have soft X-ray luminosities of $\sim 10^{41}$–10^{44} erg s^{-1} (K. Auchettl et al. 2017; S. Gezari 2021).

3. AT2023vto is a TDE

AT2023vto was classified initially as an SLSN-II based on the claimed detection of Hβ emission (F. Poidevin et al. 2023). We have shown that our optical spectrum is instead dominated by He II λ4686, and no Hβ emission is detected. The velocity width of the emission feature, $\approx 3.9 \times 10^4$ km s^{-1}, is much broader than typically observed in SNe, but it is more in line with velocities observed in TDE spectra (P. Charalampopoulos et al. 2022; E. J. Parkinson et al. 2022); see Figure 5. The line center is blueshifted relative to the rest frame of He II by $\approx 1.11 \times 10^4$ km s^{-1}, which is higher than in previous TDE-He events, but at least one other event has a comparable blueshift (Figure 4).

Another strong indication of a TDE origin is the persistent and blue $g - r \approx -0.4$ mag color of AT2023vto during both the rise and decline phases of the light curve. Such persistent blue colors are observed in other TDEs (E. Hammerstein et al. 2023), with a typical range of about -0.5 to 0 mag (mean of ≈ -0.4 mag). On the other hand, this is in contradiction to Type IIn SNe or SLSNe-II, which show a typical rapid transition from blue color on the rise to a red color ($g - r \gtrsim 0$ mag) postpeak (e.g., C. Inserra et al. 2018; D. Hiramatsu et al. 2024).

Finally, we consider the location of AT2023vto relative to its underlying host galaxy. The centroid position of the galaxy lies at the same pixel (pixel size = 0.″25) in PS1 as the centroid location of AT2023vto. We performed relative astrometry between the LCO and PanSTARRS DR1 images to determine the offset between AT2023vto and its host galaxy. We find a

[10] https://www.swift.ac.uk/user_objects/index.php
[11] Via the NASA HEASARC $N_{\rm H}$ tool: https://heasarc.gsfc.nasa.gov/cgi-bin/Tools/w3nh/w3nh.pl.
[12] Via the NASA HEASARC WebPIMMS: https://heasarc.gsfc.nasa.gov/cgi-bin/Tools/w3pimms/w3pimms.pl.

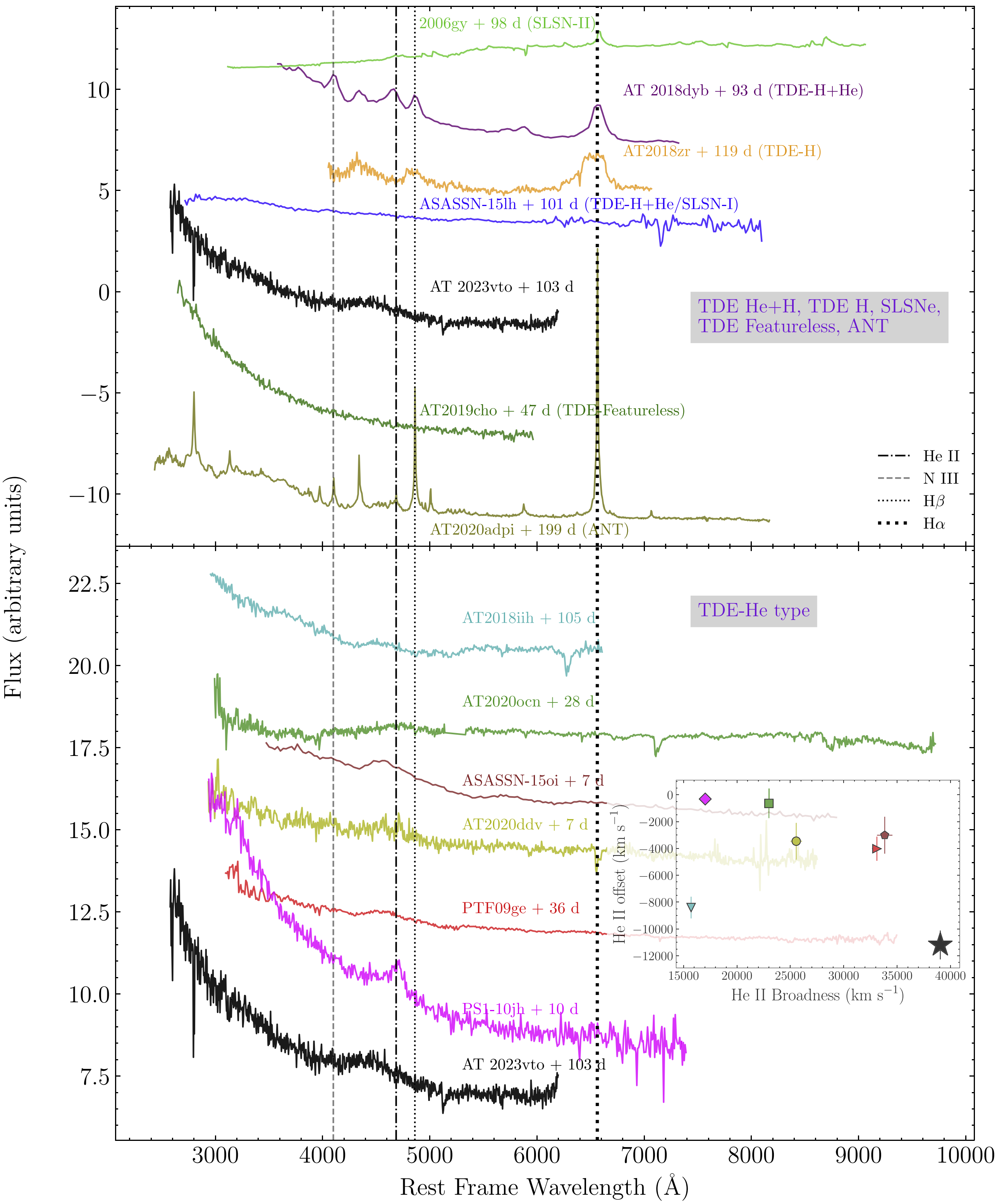

Figure 5. Top: the optical spectrum of AT2023vto compared to all TDE types (H, H+He, He, "featureless"), SLSN-II, ANT, and ASASSAN-15lh; the quoted phases are relative to the discovery date of each event. Bottom: a comparison to all other TDE-He events found to date. AT2023vto exhibits a bluer continuum compared to the other TDE-He (matched only by PS1-10jh but at a much earlier phase of its evolution). The width and blueshift of the He II λ4686 line of AT2023vto compared to the other TDE-He events are shown in the inset (colors match those of the spectra in the main panel). AT2023vto exhibits the largest velocity width and blueshift, although neither quantity is completely unprecedented in previous TDE-HE events. Comparison data from N. Smith et al. (2007), I. Arcavi et al. (2014), T. W. S. Holoien et al. (2016a, 2019a), S. Dong et al. (2016), G. Leloudas et al. (2019), S. van Velzen et al. (2021a), and P. Wiseman et al. (2024).

negligible offset of 0.″13 ± 0.″12; see Figure 1. The offset uncertainty of 0.″12 corresponds to a projected physical distance uncertainty of ≈0.7 kpc at the redshift of AT2023vto.

To summarize, the spectroscopic identification of a broad He II emission line, combined with the long duration, large peak luminosity, persistent blue $g-r$ color, and a location

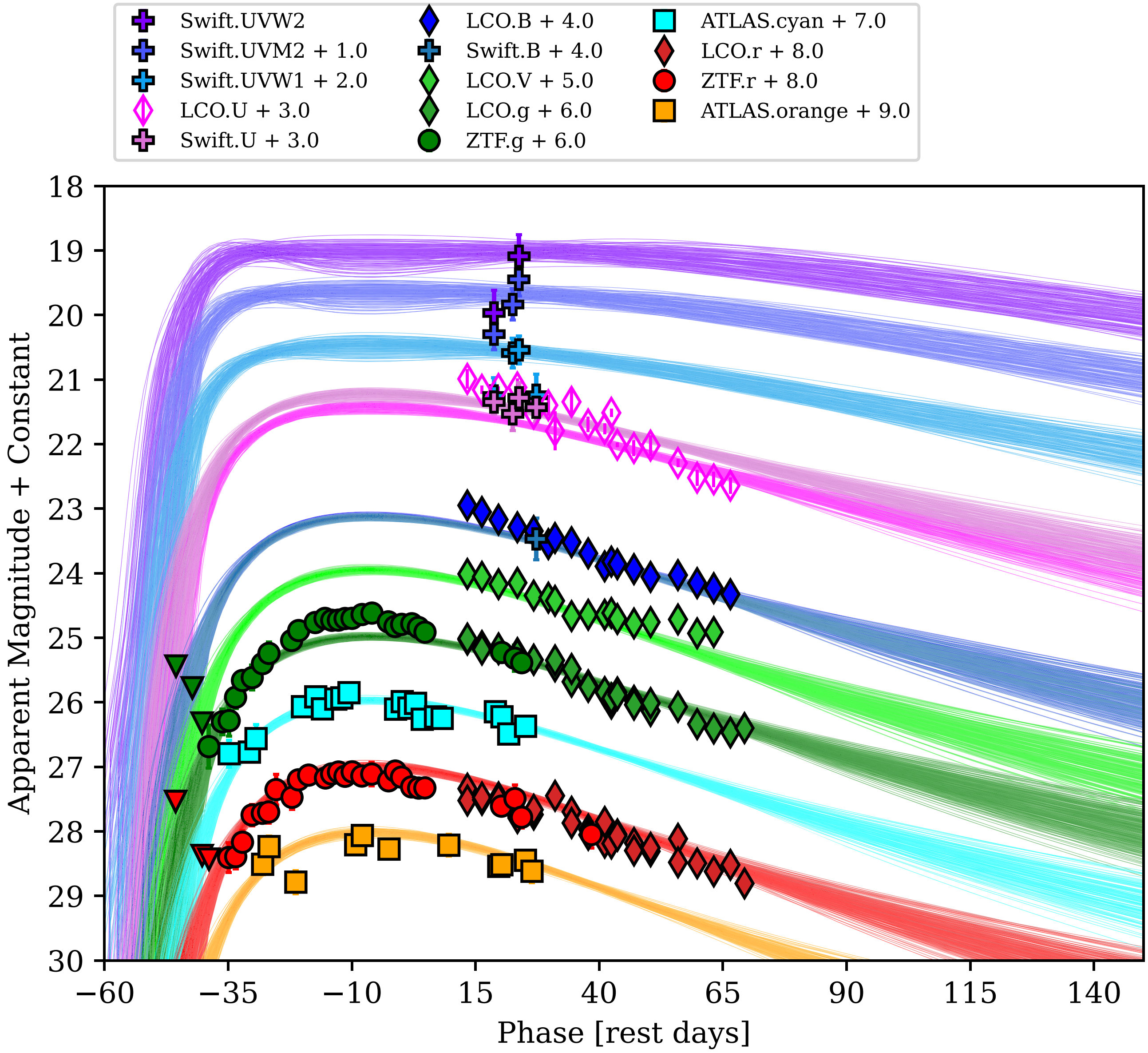

Figure 6. Multiband MOSFiT TDE model light curves for AT2023vto. We note that the LCO U-band data (open symbols) were not used in the fit, but their inclusion does not change the resulting model parameters. The best-fit model parameters are listed in Table 2.

consistent with the nucleus of its host galaxy, all indicate that AT2023vto is a TDE-He event.

4. Light-curve Modeling

Having identified AT2023vto as a TDE, we now turn to modeling its light curves with the MOSFiT Python package, which uses a Markov Chain Monte Carlo method to model the light curves of transients powered by various energy sources (J. Guillochon et al. 2017). The MOSFiT TDE model calculates the luminosity of the system by converting the fallback accretion rate of the disrupted stellar material to radiation (via an efficiency parameter). The model includes several parameters: the mass of the black hole ($M_{\rm BH}$); the mass of the disrupted star (M_*); the scaled impact parameter (b), accounting for the star's polytropic index and the bound mass fraction such that a value of $b = 1$ implies a full disruption; the efficiency of fallback accretion to radiation conversion (ϵ); the photosphere power-law constant ($R_{\rm ph,0}$) and exponent (l); and the viscous time ($T_{\rm viscous}$), which governs the formation rate of the accretion disk. Additionally, the model assumes a blackbody spectral energy distribution to determine the brightness in each band. The model is based on B. Mockler et al. (2019), where further details are provided. To model the observed light curves, we used the emcee ensemble sampler (D. Foreman-Mackey et al. 2013) with 200 walkers and 20,000 steps to ensure convergence of the model with a potential scale reduction factor (PSRF) of <1.1.

In Figure 6, we plot the best-fit model light-curve realizations in the optical and UV bands, and we list the resulting best-fit parameters with 1σ confidence intervals in Table 2. The model indicates that AT2023vto resulted from the disruption of an $\approx 8.2\,M_\odot$ star by a $\approx 10^7\,M_\odot$ black hole. The latter is in good agreement with the estimated value from the host galaxy stellar mass (Section 2.2). The estimated disruption time is ≈ 20 days prior to the initial ZTF detection. The normalized impact parameter is $b \approx 0.53$, and the efficiency is

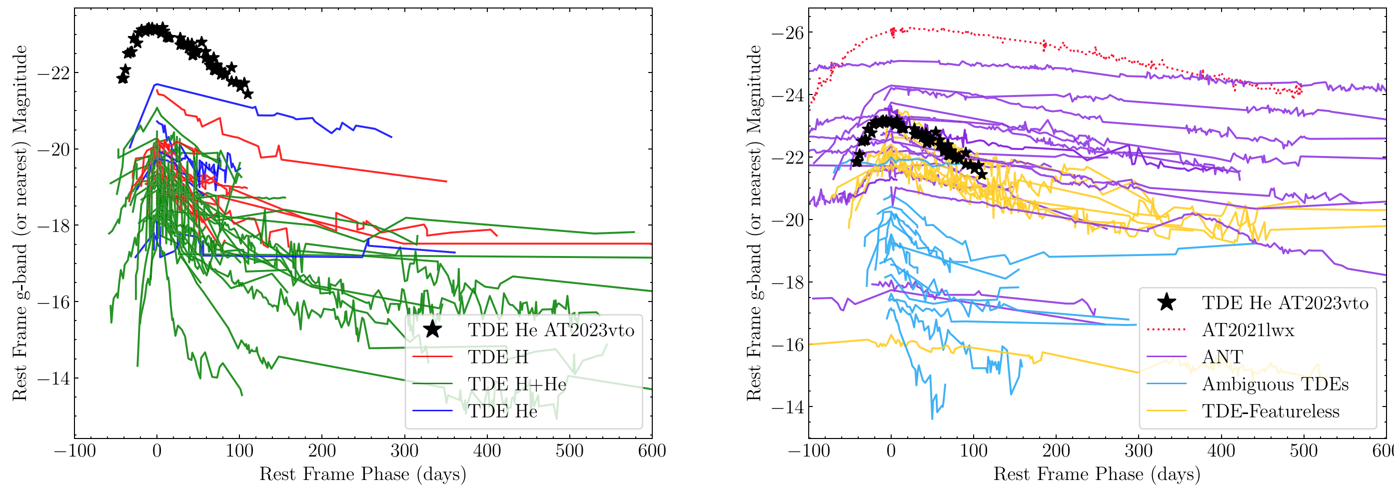

Figure 7. Left: a comparison of the rest-frame g-band light curve of AT2023vto (black stars) to the classical TDE sample, consisting of TDE-H (red), TDE-H+He (green), and TDE-He (blue). AT2023vto is the brightest among this population of spectroscopically classified TDEs, outshining the second brightest event by ≈1.5 mag and the median by ≈4 mag. Right: a comparison of AT2023vto's rest-frame g-band light curve to putative or possible TDEs, including featureless events, ambiguous events, and ANTs. AT2023vto is at the bright end of the featureless TDEs (yellow) and at the mean of the ANT population. Comparison data from S. Gezari et al. (2006), R. Chornock et al. (2014), S. van Velzen & G. R. Farrar (2014), I. Arcavi et al. (2014), T. W.-S. Holoien et al. (2014), T. W. S. Holoien et al. (2016b, 2016a), S. Dong et al. (2016), T. Hung et al. (2017), P. K. Blanchard et al. (2017), N. Blagorodnova et al. (2017), Ł. Wyrzykowski et al. (2017), S. van Velzen (2018), T. W. S. Holoien et al. (2019b), M. Nicholl et al. (2019), S. Gomez et al. (2020), P. Short et al. (2020), M. Nicholl et al. (2020), I. Arcavi et al. (2020), I. Perez-Fournon et al. (2020), J. Nordin et al. (2020), S. van Velzen et al. (2021a), T. Hung et al. (2021), G. Cannizzaro et al. (2021), Y. Yao et al. (2021a, 2021b), C. Fremling (2021), T. Wevers et al. (2022), X.-L. Liu et al. (2022), Y. Yao et al. (2022), P. Ramsden et al. (2022), M. Nicholl et al. (2022), E. Hammerstein et al. (2023), S. Gomez et al. (2023), Y. Yao et al. (2023), A. J. Goodwin et al. (2023), Y. Yao (2023), J. J. Somalwar et al. (2023), N. Sarin & B. D. Metzger (2024), P. Wiseman et al. (2024), J. T. Hinkle et al. (2024), and J. T. Hinkle (2024).

Table 2
Posterior Distribution of the TDE Model Parameters from MOSFiT

Parameter	Range	Log-prior	Posterior
M_* ($M_\odot$)	[0.01, 100]	False	$8.29^{+4.59}_{-3.55}$
$M_{\rm BH}$ ($M_\odot$)	[10^4, 10^{10}]	True	$7.02^{+0.07}_{-0.06}$
$t_{\rm exp}$ (days)	[−100, 0]	False	$-23.65^{+5.16}_{-5.92}$
b	[0, 2]	False	$0.67^{+0.12}_{-0.11}$
ϵ	[1×10^{-4}, 0.4]	True	$-2.27^{+0.25}_{-0.22}$
$T_{\rm viscous}$ (days)	[0.01, 10^3]	True	$-1.15^{+1.36}_{-1.35}$
$R_{\rm ph,0}$	[10^{-4}, 10^4]	True	$0.93^{+0.09}_{-0.06}$
$l_{\rm ph}$	[0, 4]	False	$1.36^{+0.30}_{-0.18}$
$n_{\rm H,host}$ (cm^{-2})	[10^{16}, 10^{23}]	True	$17.51^{+1.16}_{-1.04}$
$A_{\rm V}$ (mag)	...	False	$0.0002^{+0.002}_{-0.0002}$
σ	[10^{-3}, 100]	True	$-0.77^{+0.03}_{-0.03}$

$\epsilon \approx 0.006$. As expected, the best-fit host galaxy extinction is consistent with zero.

The model provides an overall good fit to the optical and UV data. We note that it does not fully capture the light-curve behavior near the peak in the g band (the model is overall smoother than the data). This is potentially due to the simplified nature of the TDE model; for example, the models are calibrated for lower-mass stars than inferred for AT2023vto, and it is possible that high-mass stars have somewhat different internal structures, which will affect the debris dynamics during disruption (R. Kippenhahn et al. 2013; J. Guillochon & E. Ramirez-Ruiz 2015).

The best-fit model from MOSFiT results in a peak bolometric luminosity of $L_{p,\rm bol} = (7.7 \pm 0.4) \times 10^{44}$ erg s^{-1}, a blackbody temperature of $T_{p,\rm BB} = 13{,}560 \pm 378$ K, and a blackbody radius of $R_{p,\rm BB} = (5.6 \pm 0.3) \times 10^{15}$ cm. The radiated energy integrated from the estimated disruption time to the time of the last available observation is $E_{\rm rad} \approx 1.8 \times 10^{52}$ erg.

5. Discussion

5.1. Comparison to the Light Curves and Models of Optical TDEs

In this section, we compare AT2023vto to the optical TDE population and to other possibly related transients using its observed light curve and spectroscopic properties, as well as the inferred physical parameters from MOSFiT modeling compared to those of the optical TDE population (S. Gomez et al., 2024, in preparation)

In Figure 7 we compare the rest-frame g-band light curve of AT2023vto to a sample of 72 optical TDEs and potential TDEs (see references in the caption of Figure 7); for the comparison objects, we use the nearest available filter to rest-frame g band. We divide the comparison sample into two categories: (i) classical TDEs, where the TDE classification is based on spectroscopic features (e.g., H and/or He lines); and (ii) putative or potential TDEs, where the spectra are either featureless or exhibit spectral features that are distinct from classical TDEs (e.g., narrow emission lines as in ANTs) but which are consistent with a nuclear origin. The latter category includes events with featureless spectra that are classified as a TDE due to their persistent blue colors, TDE-like light-curve properties, and coincidence with the nuclei of their host galaxies (S. van Velzen et al. 2021b; M. Nicholl et al. 2022; E. Hammerstein et al. 2023); the ambiguous event ASASSAN-15lh, which was claimed to be both an SLSN and a TDE (P. J. Brown et al. 2016; S. Dong et al. 2016; G. Leloudas et al. 2016); ANTs, which spatially coincide with their host galaxy nuclei but are spectrally distinct from TDEs (E. Kankare et al. 2017; J. T. Hinkle et al. 2024; P. Wiseman et al. 2024); and ambiguous events, which include a variety of transients with a

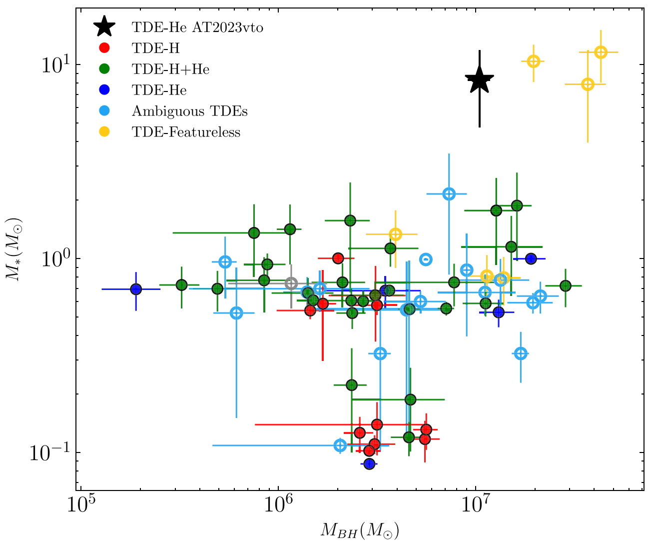

Figure 8. Inferred disrupted star mass (M_*) vs. black hole mass ($M_{\rm BH}$) from MOSFiT model fits of AT2023vto (black star) and optical TDEs, including the H (red), H+He (green), and He (purple) categories, as well as featureless (open yellow) and ambiguous events (open blue). AT2023vto stands out in this parameter space with an unusually high stellar mass and relatively large black hole mass. A few of the featureless TDEs seem to reside in the same region of parameter space as AT2023vto and indeed exhibit similar light curves (right panel of Figure 7).

nuclear origin that are referred to as ambiguous/unknown in the TDE literature (S. van Velzen et al. 2021b; M. Nicholl et al. 2022; E. Hammerstein et al. 2023; Y. Yao et al. 2023).

We find that AT2023vto is the brightest among all of the classical spectroscopically classified TDEs, outshining the second brightest event by ≈1.5 mag and the median of the population (−19.7 ± 0.9 mag) by ≈4 mag. On the other hand, AT2023vto exhibits a similar rise time (≈50 days) to the optical TDE sample (with ≈30–60 days), as well as a similar decline rate (Figure 7).

Next, we compare the light curve of AT2023vto to the putative TDEs and ANTs. AT2023vto is more luminous than all of the "ambiguous" TDE events and also exceeds the luminosities of the "featureless" events, although some of those are comparable in brightness. On the other hand, AT2023vto is comparable to the *mean* of the ANT population, but those generally have longer durations and extend about 2 mag brighter.

In Figure 8, we compare the key inferred physical parameters of AT2023vto—M_* and $M_{\rm BH}$—to the classical TDE sample and featureless possible TDEs. The comparison events are modeled in exactly the same way as our MOSFiT model for AT2023vto. As expected from its high luminosity, we find that AT2023vto stands out in terms of the disrupted star mass of $M_* \approx 8.2\ M_\odot$ from the rest of the TDE population, which spans $M_* \approx 0.1$–$2\ M_\odot$ with a mean of $\langle M_* \rangle = 0.64 \pm 0.46\ M_\odot$. We also find that $M_{\rm BH} \approx 10^7\ M_\odot$ in AT2023vto is at the massive end of the distribution, which spans $M_{\rm BH} \approx 10^{5.5}$–$10^{7.5}\ M_\odot$, with a mean of $\langle M_{\rm BH} \rangle \approx 10^{6.5}\ M_\odot$. For the black hole mass in AT2023vto, its peak bolometric luminosity corresponds to $\approx 0.65\ L_{\rm Edd}$, which is in the upper range for optical TDEs (P. K. Blanchard et al. 2017; T. Hung et al. 2017; B. Mockler et al. 2019; T. H. T. Wong et al. 2022). Finally, the scaled impact parameter in AT2023vto, $b \approx 0.67$, is somewhat lower than for other TDE-He events, with $b \sim 1$ (M. Nicholl et al. 2022).

While AT2023vto resides in a distinct part of the $M_* - M_{\rm BH}$ phase space than classical TDEs, some of the featureless events (AT2018jbv, AT2020acka, AT2020riz) occupy a similar parameter space, with $M_* \sim 10\ M_\odot$ and $M_{\rm BH} \sim 10^{7.5}\ M_\odot$. Similarly, some of the similar, or even more luminous, ANTs than AT2023vto, if interpreted as TDEs, have been argued to result from massive stars, $M_* \sim 4.5$–$90\ M_\odot$, disrupted by similarly massive black holes, $M_{\rm BH} \sim 10^{7.2}$–$10^{8.7}\ M_\odot$ (B. Mockler et al. 2022; J. T. Hinkle et al. 2024; P. Wiseman et al. 2024), even though the shorter lifetime and initial mass function of Sun-like stars near galactic nuclei generally imply that the TDEs of massive star events should be rare (P. Wiseman et al. 2023).

5.2. Comparison to the Spectra of Optical TDEs

In Figure 5, we compare the optical spectrum of AT2023vto to that of other TDE-He events, as well as to that of ambiguous or potential TDEs (e.g., ASASSN-15lh, ANTs); we compare these at the nearest epoch to ∼100 days postdiscovery available on WISeREP (O. Yaron et al. 2021) to match the epoch of the AT2023vto spectrum.

The spectrum of AT2023vto is broadly similar to that of the other TDE-He events, with the closest analog being PS1-10jh (albeit at an earlier epoch of about 10 days postdiscovery). AT2023vto has a bluer continuum than the other TDE-He. In the inset of Figure 5, we plot the He II λ4686 line width versus blueshift for AT2023vto and the six comparison TDE-He events. We find that AT2023vto exhibits the largest line width and the largest blueshift, although some TDE-He events have comparable line widths ($\approx 3 \times 10^4$ km s^{-1}) or blueshift ($\approx 8 \times 10^3$ km s^{-1}). We note that none of the TDE-He events exhibit a redshift of the He II line, as opposed to the trend seen in the Balmer lines of TDE-H and TDE-H+He events (P. Charalampopoulos et al. 2022).

While AT2023vto is comparable in peak luminosity to the mean of the ANT population, the latter has clearly distinct spectra compared to AT2023vto and classical TDEs, marked by much narrower Balmer lines, as well as narrow lines of O I, [O II], and [O III] (J. T. Hinkle et al. 2024; P. Wiseman et al. 2024). The Balmer line widths are ≲3000 km s^{-1} compared to ≳10,000 km s^{-1} for classical TDEs. P. Wiseman et al. (2024) found that 8 out of 10 ANTs in their sample show a narrow [O III] λ5007 line, which is commonly present in AGNs and star-forming galaxy spectra and is indicative of low-density ionized gas. One possibility is that ANTs occur in preexisting AGNs, explaining their narrower lines from the AGN environment. On the other hand, the spectral properties of AT2023vto match those of the classical TDE-He population, despite a potential similarity in disrupted star mass and black hole mass (Section 5.1), suggesting that it arose from a quiescent SMBH.

6. Conclusions

We presented photometric and spectroscopic observations of AT2023vto, a luminous transient at $z = 0.4846$ that we have shown to be a TDE based on the identification of a broad He II λ4686 emission line, persistent $g - r \approx -0.4$ mag color during the long rise and decline of the light curve, and a location consistent with the nucleus of its underlying host galaxy. A comparison to the spectra of other TDEs indicates that AT2023vto is a TDE-He event. We reach the following conclusions based on the observed properties of AT2023vto and the modeling of its light curves:

1. The peak absolute magnitude of $m_g \approx -23.2$ makes AT2023vto the most luminous classical TDE observed to date, by ≈1.5 mag compared to the second brightest TDE and by ≈3.5 mag (≈4 standard deviation) compared to the median of the TDE population.
2. The peak brightness of AT2023vto is similar to some putative TDEs, namely, some "featureless" events and the mean of the ANT population. However, its TDE-He spectrum is distinct from those of ANTs (which are dominated by narrow lines, including Balmer lines) and featureless events (which lack any spectroscopic features).
3. The He II λ4686 line in AT2023vto exhibits the largest combination of velocity width ($\approx 3.90 \times 10^4$ km s^{-1}) and blueshift (-1.11×10^4 km s^{-1}) of any TDE-He event to date, but neither value on its own is unprecedented.
4. Modeling of the light curves indicates that AT2023vto was caused by the disruption of a $\approx 8\ M_\odot$ star by a $\approx 10^7$ $M_\odot$ black hole (the black hole mass is in good agreement with the value inferred based on the host galaxy mass). This combination is unique among optical TDEs; the star mass is about 5 times larger than the most massive stars in previous TDEs and about 14 times larger than the mean of the population ($\langle M_* \rangle \approx 0.64$). Similar parameters are only found in models of the putative "featureless" TDEs, as well as by TDE model fits for ANTs (T. W. S. Holoien et al. 2022; J. T. Hinkle et al. 2024; D. Hiramatsu et al. 2024; P. Wiseman et al. 2024).

AT2023vto is a classical TDE in terms of its observed photometric and spectroscopic properties while having been caused by the disruption of a much more massive star than the general TDE population, similar to those inferred in the TDE model fits to luminous ANTs. Thus, AT2023vto may be a link between the two populations. The majority of ANTs exhibit different spectra than classical TDEs, dominated by narrow Balmer and oxygen lines. It is possible that both AT2023vto and the luminous ANTs are caused by massive star disruptions, with the latter occurring in active galactic nuclei and AT2023vto occurring in a dormant SMBH.

The large luminosity and inferred star mass in AT2023vto provide an opportunity to study the extreme end of the TDE luminosity function and the impact of massive star disruptions. With the upcoming Rubin Observatory/LSST, we anticipate that AT2023vto-like events will be detectable to $z \sim 3$ and would, therefore, also probe quiescent SMBHs to much larger redshifts than the bulk of the TDE population. Along with an increase in the detection rate and characterization of ANTs, we expect that such observations will shed light on the connection between luminous TDEs and ANTs.

Acknowledgments

We thank Brenna Mockler and Conor Ransome for the useful discussions. The Berger Time-Domain research group at Harvard is supported by NSF and NASA grants. The LCO supernova group is supported by NSF grants AST-1911151 and AST-1911225.

Observations reported here were obtained at the MMT Observatory, a joint facility of the Smithsonian Institution and the University of Arizona. This Letter uses data products produced by the OIR Telescope Data Center, supported by the Smithsonian Astrophysical Observatory.

This work makes use of observations from the Las Cumbres Observatory global telescope network. The authors wish to recognize and acknowledge the very significant cultural role and reverence that the summit of Haleakal has always had within the indigenous Hawaiian community. We are most fortunate to have the opportunity to conduct observations from the mountain.

We thank the support of the staff at the Neil Gehrels Swift Observatory.

This work has made use of data from the Zwicky Transient Facility (ZTF). ZTF is supported by NSF grant No. AST-1440341 and a collaboration including Caltech, IPAC, the Weizmann Institute for Science, the Oskar Klein Center at Stockholm University, the University of Maryland, the University of Washington, Deutsches Elektronen-Synchrotron and Humboldt University, Los Alamos National Laboratories, the TANGO Consortium of Taiwan, the University of Wisconsin–Milwaukee, and Lawrence Berkeley National Laboratories. Operations are conducted by COO, IPAC, and UW. The ZTF forced photometry service was funded under the Heising-Simons Foundation grant No. 12540303 (PI: Graham).

This work has made use of data from the Asteroid Terrestrial-impact Last Alert System (ATLAS) project. The ATLAS project is primarily funded to search for near-Earth asteroids through NASA grants NN12AR55G, 80NSSC18K0284, and 80NSSC18K1575; byproducts of the NEO search include images and catalogs from the survey area. This work was partially funded by Kepler/K2 grant J1944/80NSSC19K0112 and HST GO-15889 and STFC grants ST/T000198/1 and ST/S006109/1. The ATLAS science products have been made possible through the contributions of the University of Hawaii Institute for Astronomy, the Queens University Belfast, the Space Telescope Science Institute, the South African Astronomical Observatory, and the Millennium Institute of Astrophysics (MAS), Chile.

The PS1 and the PS1 public science archives have been made possible through contributions by the Institute for Astronomy; the University of Hawaii; the Pan-STARRS Project Office; the Max Planck Society and its participating institutes—the Max Planck Institute for Astronomy, Heidelberg, and the Max Planck Institute for Extraterrestrial Physics, Garching; Johns Hopkins University; Durham University; the University of Edinburgh; the Queens University Belfast; the Harvard-Smithsonian Center for Astrophysics; the Las Cumbres Observatory Global Telescope Network Incorporated; the National Central University of Taiwan; the Space Telescope Science Institute, NASA under grant No. NNX08AR22G, issued through the Planetary Science Division of the NASA Science Mission Directorate, NSF grant No. AST- 1238877; the University of Maryland; Eotvos Lorand University; the Los Alamos National Laboratory; and the Gordon and Betty Moore Foundation.

This research has made use of the NASA Astrophysics Data System (ADS), the NASA/IPAC Extragalactic Database (NED), and NASA/IPAC Infrared Science Archive (IRSA; which is funded by NASA and operated by the California Institute of Technology) and IRAF (which is distributed by the National Optical Astronomy Observatory, NOAO, operated by the Association of Universities for Research in Astronomy, AURA, Inc., under cooperative agreement with the NSF).

TNS is supported by funding from the Weizmann Institute of Science, as well as grants from the Israeli Institute for Advanced Studies and the European Union via ERC grant No. 725161.

Facilities: ATLAS, LCO, Swift (XRT and UVOT), ZTF, MMT.

Software: astropy (Astropy Collaboration et al. 2013, 2018, 2022), SExtractor (E. Bertin & S. Arnouts 1996) NumPy (T. E. Oliphant 2015), photutils (L. Bradley et al. 2022), PyRAF (Science Software Branch at STScI 2012), SciPy (P. Virtanen et al. 2020) and MOSFiT (J. Guillochon et al. 2017).

ORCID iDs

Harsh Kumar https://orcid.org/0000-0003-0871-4641
Edo Berger https://orcid.org/0000-0002-9392-9681
Daichi Hiramatsu https://orcid.org/0000-0002-1125-9187
Sebastian Gomez https://orcid.org/0000-0001-6395-6702
Peter K. Blanchard https://orcid.org/0000-0003-0526-2248
Yvette Cendes https://orcid.org/0000-0001-7007-6295
Estefania Padilla Gonzalez https://orcid.org/0000-0003-0209-9246
Curtis McCully https://orcid.org/0000-0001-5807-7893
Giacomo Terreran https://orcid.org/0000-0003-0794-5982

References

Alexander, K. D., van Velzen, S., Horesh, A., & Zauderer, B. A. 2020, SSRv, 216, 81
Anderson, J. P., Dessart, L., Gutierrez, C. P., et al. 2014, MNRAS, 441, 671
Arcavi, I., Burke, J., Nyiha, I., et al. 2020, TNSCR, 2020-3228, 1
Arcavi, I., Gal-Yam, A., Sullivan, M., et al. 2014, ApJ, 793, 38
Astropy Collaboration, Price-Whelan, A. M., Lim, P. L., et al. 2022, ApJ, 935, 167
Astropy Collaboration, Robitaille, T. P., Tollerud, E. J., et al. 2013, A&A, 558, A33
Auchettl, K., Guillochon, J., & Ramirez-Ruiz, E. 2017, ApJ, 838, 149
Bellm, E. 2014, in The Third Hot-wiring the Transient Universe Workshop, ed. P. R. Wozniak et al., 27
Bellm, E. C., Kulkarni, S. R., Graham, M. J., et al. 2019, PASP, 131, 018002
Berger, E., Zauderer, A., Pooley, G. G., et al. 2012, ApJ, 748, 36
Bertin, E., & Arnouts, S. 1996, A&AS, 117, 393
Blagorodnova, N., Gezari, S., Hung, T., et al. 2017, ApJ, 844, 46
Blanchard, P. K., Nicholl, M., Berger, E., et al. 2017, ApJ, 843, 106
Bradley, L., Sipőcz, B., Robitaille, T., et al. 2022, astropy/photutils: v1.5.0, Zenodo, doi:10.5281/zenodo.6825092
Brown, G. C., Levan, A. J., Stanway, E. R., et al. 2017, MNRAS, 472, 4469
Brown, P. J., Breeveld, A. A., Holland, S., Kuin, P., & Pritchard, T. 2014, Ap&SS, 354, 89
Brown, P. J., Holland, S. T., Immler, S., et al. 2009, AJ, 137, 4517
Brown, P. J., Yang, Y., Cooke, J., et al. 2016, ApJ, 828, 3
Brown, T. M., Baliber, N., Bianco, F. B., et al. 2013, PASP, 125, 1031
Cannizzaro, G., Wevers, T., Jonker, P. G., et al. 2021, MNRAS, 504, 792
Cendes, Y., Berger, E., Alexander, K. D., et al. 2024, ApJ, 971, 185
Charalampopoulos, P., Leloudas, G., Malesani, D. B., et al. 2022, A&A, 659, A34
Chornock, R., Berger, E., Gezari, S., et al. 2014, ApJ, 780, 44
Collaboration, Astropy, Price-Whelan, A. M., Sipőcz, B. M., et al. 2018, AJ, 156, 123
Dong, S., Shappee, B. J., Prieto, J. L., et al. 2016, Sci, 351, 257
Drake, A. J., Djorgovski, S. G., Mahabal, A., et al. 2011, ApJ, 735, 106
Evans, C. R., & Kochanek, C. S. 1989, ApJL, 346, L13
Evans, P. A., Beardmore, A. P., Page, K. L., et al. 2007, A&A, 469, 379
Evans, P. A., Beardmore, A. P., Page, K. L., et al. 2009, MNRAS, 397, 1177
Fabricant, D., Fata, R., Epps, H., et al. 2019, PASP, 131, 075004
Fitzpatrick, E. L. 1999, PASP, 111, 63
Foreman-Mackey, D., Hogg, D. W., Lang, D., & Goodman, J. 2013, PASP, 125, 306
Förster, F., Cabrera-Vives, G., Castillo-Navarrete, E., et al. 2021, AJ, 161, 242
Fremling, C. 2021, TNSTR, 2021-3208, 1
Fremling, C. 2023, TNSTR, 2023-2714, 1
Gehrels, N., Chincarini, G., Giommi, P., et al. 2004, ApJ, 611, 1005
Gezari, S. 2021, ARA&A, 59, 21
Gezari, S., Martin, D. C., Milliard, B., et al. 2006, ApJL, 653, L25
Gomez, S., Nicholl, M., Short, P., et al. 2020, MNRAS, 497, 1925
Gomez, S., Villar, V. A., Berger, E., et al. 2023, ApJ, 949, 113
Goodwin, A. J., Alexander, K. D., Miller-Jones, J. C. A., et al. 2023, MNRAS, 522, 5084
Greene, J. E., Strader, J., & Ho, L. C. 2020, ARA&A, 58, 257
Guillochon, J., Nicholl, M., Villar, V. A., et al., 2017 MOSFiT: Modular Open-Source Fitter for Transients, Astrophysics Source Code Library, ascl:1710.006
Guillochon, J., & Ramirez-Ruiz, E. 2015, ApJ, 798, 64
Hammerstein, E., van Velzen, S., Gezari, S., et al. 2023, ApJ, 942, 9
Henden, A. A., Templeton, M., Terrell, D., et al. 2016, yCat, II/336
HI4PI Collaboration, Ben Bekhti, N., Flöer, L., et al. 2016, A&A, 594, A116
Hinkle, J. T. 2024, MNRAS, 531, 2603
Hinkle, J. T., Shappee, B. J., Auchettl, K., et al. 2024, arXiv:2405.08855
Hiramatsu, D., Matsumoto, T., Berger, E., et al. 2024, ApJ, 964, 181
Holoien, T. W. S., Huber, M. E., Shappee, B. J., et al. 2019a, ApJ, 880, 120
Holoien, T. W. S., Kochanek, C. S., Prieto, J. L., et al. 2016a, MNRAS, 463, 3813
Holoien, T. W. S., Kochanek, C. S., Prieto, J. L., et al. 2016b, MNRAS, 455, 2918
Holoien, T. W. S., Neustadt, J. M. M., Vallely, P. J., et al. 2022, ApJ, 933, 196
Holoien, T. W.-S., Prieto, J. L., Bersier, D., et al. 2014, MNRAS, 445, 3263
Holoien, T. W. S., Vallely, P. J., Auchettl, K., et al. 2019b, ApJ, 883, 111
Howell, D. A. & Global Supernova Project 2017, AAS Meeting Abstracts, 230, 318.03
Hung, T., Cenko, S. B., Roth, N., et al. 2019, ApJ, 879, 119
Hung, T., Foley, R. J., Veilleux, S., et al. 2021, ApJ, 917, 9
Hung, T., Gezari, S., Blagorodnova, N., et al. 2017, ApJ, 842, 29
Inserra, C., Smartt, S. J., Gall, E. E. E., et al. 2018, MNRAS, 475, 1046
Kankare, E., Kotak, R., Mattila, S., et al. 2017, NatAs, 1, 865
Kippenhahn, R., Weigert, A., & Weiss, A. 2013, Stellar Structure and Evolution (Berlin: Springer)
Leja, J., Johnson, B. D., Conroy, C., van Dokkum, P. G., & Byler, N. 2017, ApJ, 837, 170
Leloudas, G., Dai, L., Arcavi, I., et al. 2019, ApJ, 887, 218
Leloudas, G., Fraser, M., Stone, N. C., et al. 2016, NatAs, 1, 0002
Liu, X.-L., Dou, L.-M., Chen, J.-H., & Shen, R.-F. 2022, ApJ, 925, 67
McMullin, J. P., Waters, B., Schiebel, D., Young, W., & Golap, K. 2007, in ASP Conf. Ser. 376, Astronomical Data Analysis Software and Systems XVI, ed. R. A. Shaw, F. Hill, & D. J. Bell (Melville, NY: ASP), 127
Mockler, B., Guillochon, J., & Ramirez-Ruiz, E. 2019, ApJ, 872, 151
Mockler, B., Twum, A. A., Auchettl, K., et al. 2022, ApJ, 924, 70
Neustadt, J. M. M., Holoien, T. W.-S., Kochanek, C. S., et al. 2020, MNRAS, 494, 2538
Nicholl, M., Blanchard, P. K., Berger, E., et al. 2019, MNRAS, 488, 1878
Nicholl, M., Lanning, D., Ramsden, P., et al. 2022, MNRAS, 515, 5604
Nicholl, M., Wevers, T., Oates, S. R., et al. 2020, MNRAS, 499, 482
Nordin, J., Brinnel, V., Giomi, M., et al. 2020, TNSTR, 2020-3332, 1
Oliphant, T. E. 2015, Guide to NumPy (London: Continuum Press)
Parkinson, E. J., Knigge, C., Matthews, J. H., et al. 2022, MNRAS, 510, 5426
Perez-Fournon, I., Angel, C. J., Poidevin, F., et al. 2020, TNSTR, 2020-2500, 1
Planck Collaboration, Aghanim, N., Akrami, Y., et al. 2020, A&A, 641, A6
Poidevin, F., Pérez-Fournon, I., Geier, S., et al. 2023, TNSTR, 2023-3050, 1
Ramsden, P., Lanning, D., Nicholl, M., & McGee, S. L. 2022, MNRAS, 515, 1146
Rees, M. J. 1988, Natur, 333, 523
Roming, P. W. A., Kennedy, T. E., Mason, K. O., et al. 2005, SSRv, 120, 95
Roth, N., & Kasen, D. 2018, ApJ, 855, 54
Sarin, N., & Metzger, B. D. 2024, ApJL, 961, L19
Schlafly, E. F., & Finkbeiner, D. P. 2011, ApJ, 737, 103
Science Software Branch at STScI, 2012 PyRAF: Python alternative for IRAF, Astrophysics Source Code Library, ascl:1207.011
Shingles, L., Smith, K. W., Young, D. R., et al. 2021, TNSAN, 7, 1
Short, P., Nicholl, M., Lawrence, A., et al. 2020, MNRAS, 498, 4119
Smith, N., Li, W., Foley, R. J., et al. 2007, ApJ, 666, 1116
Somalwar, J. J., Ravi, V., Yao, Y., et al. 2023, arXiv:2310.03782
Stetson, P. B. 2000, PASP, 112, 925
Subrayan, B. M., Milisavljevic, D., Chornock, R., et al. 2023, ApJL, 948, L19
Tonry, J. L., Denneau, L., Heinze, A. N., et al. 2018, PASP, 130, 064505
Valenti, S., Howell, D. A., Stritzinger, M. D., et al. 2016, MNRAS, 459, 3939
van Velzen, S. 2018, ApJ, 852, 72
van Velzen, S., & Farrar, G. R. 2014, ApJ, 792, 53
van Velzen, S., Gezari, S., Hammerstein, E., et al. 2021a, ApJ, 908, 4

van Velzen, S., Pasham, D. R., Komossa, S., Yan, L., & Kara, E. A. 2021b, SSRv, 217, 63
Virtanen, P., Gommers, R., Oliphant, T. E., et al. 2020, NatMe, 17, 261
Wevers, T., Nicholl, M., Guolo, M., et al. 2022, A&A, 666, A6
Wiseman, P., Wang, Y., Honig, S., et al. 2023, MNRAS, 522, 3992
Wiseman, P., Williams, R. D., Arcavi, I., et al. 2024, arXiv:2406.11552
Wong, T. H. T., Pfister, H., & Dai, L. 2022, ApJL, 927, L19
Wyrzykowski, Ł., Zieliński, M., & Kostrzewa-Rutkowska, Z. 2017, MNRAS, 465, L114
Yao, Y. 2023, TNSCR, 2023-2004, 1
Yao, Y., Chu, M., Das, K. K., et al. 2021a, TNSCR, 2021-3611, 1
Yao, Y., Lu, W., Guolo, M., et al. 2022, ApJ, 937, 8
Yao, Y., Ravi, V., Gezari, S., et al. 2023, ApJL, 955, L6
Yao, Y., Velzen, S. V., Perley, D., et al. 2021b, TNSCR, 2021-1632, 1
Yaron, O., Sass, A., Gal-Yam, A., & Knezevic, N. 2021, TNSAN, 142, 1
Zackay, B., Ofek, E. O., & Gal-Yam, A. 2016, ApJ, 830, 27
Zauderer, B. A., Berger, E., Margutti, R., et al. 2013, ApJ, 767, 152
Zhou, Z. Q., Liu, F. K., Komossa, S., et al. 2021, ApJ, 907, 77